Acta Geotechnica (2021) 16:1315–1330
https://doi.org/10.1007/s11440-021-01178-w

RESEARCH PAPER

Coupling simulation of microbially induced carbonate precipitation and bacterial growth using reaction–diffusion and homogenisation systems

Ibuki Nishimura[1] · Hitoshi Matsubara[2]

Received: 22 June 2020 / Accepted: 21 February 2021 / Published online: 22 March 2021

Abstract
Soil improvement techniques have been developed experimentally and empirically from various geotechnical standpoints based on physical, chemical, and biological findings. The traditional microbiological perspectives consider microbially induced soil cementation as an environment-friendly soil improvement technique. In particular, microbially induced carbonate precipitation (MICP) is recognised as an effective method with applications in real geotechnical problems. Traditionally, highly active species with carbonate-precipitating and their optimum environmental conditions have been identified through laboratory experiments and field surveys. Recently, numerical simulations considering microbial metabolic reactions have been tried for elucidating MICP. However, the mathematical and numerical evaluation of the relationship between bacterial growth and MICP requires further investigation. This study proposed a novel numerical simulation scheme for evaluating the effects of bacterial growth on stress distribution in soil micro- and macro-structure. In particular, this scheme utilised a reaction–diffusion system to determine bacterial growth and MICP in micro-structures. Further, stress and strain distributions in multi-scale structures were evaluated by a homogenisation method. Consequently, the simulation results of the calcium carbonate precipitation were 0.85–4.5 μmol/mm^3 at 10.3 h. Evidently, the model values are reasonably consistent with the experimental data. Further, the homogenisation simulations indicated that soil stabilisation could be attributed to the formation of a novel skeleton structure comprising soil particles and calcium carbonate-filled soil pores.

Keywords Coupling simulation · Homogenisation method · Microbial growth · Reaction–diffusion system

1 Introduction

Biogeotechnology is a branch of geotechnical engineering that employs ecological approaches to address geotechnical problems [27] such as liquefaction [62]. Biogeotechnology is recognised as an environment-friendly approach which is relatively low-cost compared to traditional soil improvement techniques [27] such as sand compaction piles [59, 63] and chemical grouting [21, 28].

Biogeotechnology utilises biomineralisation, i.e. the precipitation of minerals (e.g. carbonates and silica) by bacterial and/or plant metabolism [48]. Particularly, microbially induced carbonate precipitation (MICP) has been observed in both laboratory experiments and field surveys worldwide [1, 6, 9, 11, 12, 29, 42, 47, 58]. Previous studies have identified several bacterial species, such as cyanobacteria and ureolytic bacteria, that exhibit biomineralisation under specific environmental conditions such as temperature and pH. It has been reported that the metabolic reactions of ureolytic bacteria significantly affect calcium carbonate precipitation in soils [10, 20, 48, 65]. Ureolytic bacteria require urea and water [25], while cyanobacteria require sunlight, carbon dioxide, and water for their metabolic reactions [2, 16]. Notably, ureolytic bacteria

✉ Hitoshi Matsubara
matsbara@tec.u-ryukyu.ac.jp

[1] Graduate School of University of the Ryukyus, 1 Senbaru, Nishihara-cho, Nakagami-gun, Okinawa 903-0213, Japan

[2] School of Civil Engineering, University of the Ryukyus, 1 Senbaru, Nishihara-cho, Nakagami-gun, Okinawa 903-0213, Japan

have been investigated as a bio-calcification material for the improvement of sandy soils [7, 64].

Bacteria can adsorb cations (e.g. calcium ions) from the external environment owing to presence of negatively charged functional groups on their surface [15, 18]. Hence, the chemical reaction between carbonate ions (discharged during bacterial metabolism and/or produced in alkaline environment) and calcium ions (adsorbed on bacterial cell surface) results in the precipitation of calcium carbonate around bacterial cells [30, 65]. Additionally, MICP serves to bond soil particles.

Previous studies have observed MICP in soil micro-structure using scanning electron microscopy, transmission electron microscopy, and X-ray microtomography [42, 52, 57]. The process underlying MICP is illustrated in Fig. 1. Notably, calcium carbonate precipitation on the surface of soil particles is followed by the gradual filling of voids by calcium carbonate. This calcium carbonate growth enhances the stability and strength of soils. Although these results have been primarily obtained by laboratory experiments and field investigations, recent studies have focused on mathematical and numerical simulations in this regard [1, 33, 56].

Matsubara and Yamada [33] proposed a mathematical model based on a reaction–diffusion system and numerically simulated the MICP at micro-scale. The proposed model could simulate MICP on the surface of soil particles. Notably, the combination of microscopy and simulation results allowed the deductive and visual understanding of the MICP. However, this model did not consider the growth of bacterial colonies in soils; therefore, it was difficult to comprehensively elucidate the relationship between bacterial growth and MICP. In addition, no previous study has simulated the relationship between changes in soil micro-structure due to MICP and the strength development of soil micro- and macro-structure.

Notably, studies in the field of numerical/theoretical biology have investigated spatio-temporal growth and colour patterns in various creatures, insects, and bacterial colonies to develop numerical simulators of morphological patterns [34]. For instance, as indicated by a numerical logistic model, the growth of bacterial colonies generally depends on growth velocity and individual density [35]. Several models as mentioned above have been formulated based on reaction–diffusion systems [17, 34]. Therefore, models simulating the growth of bacterial colonies may have a high affinity with the MICP model proposed by [33].

In this study, we assessed the relationship between changes in soil micro-structure due to MICP and the

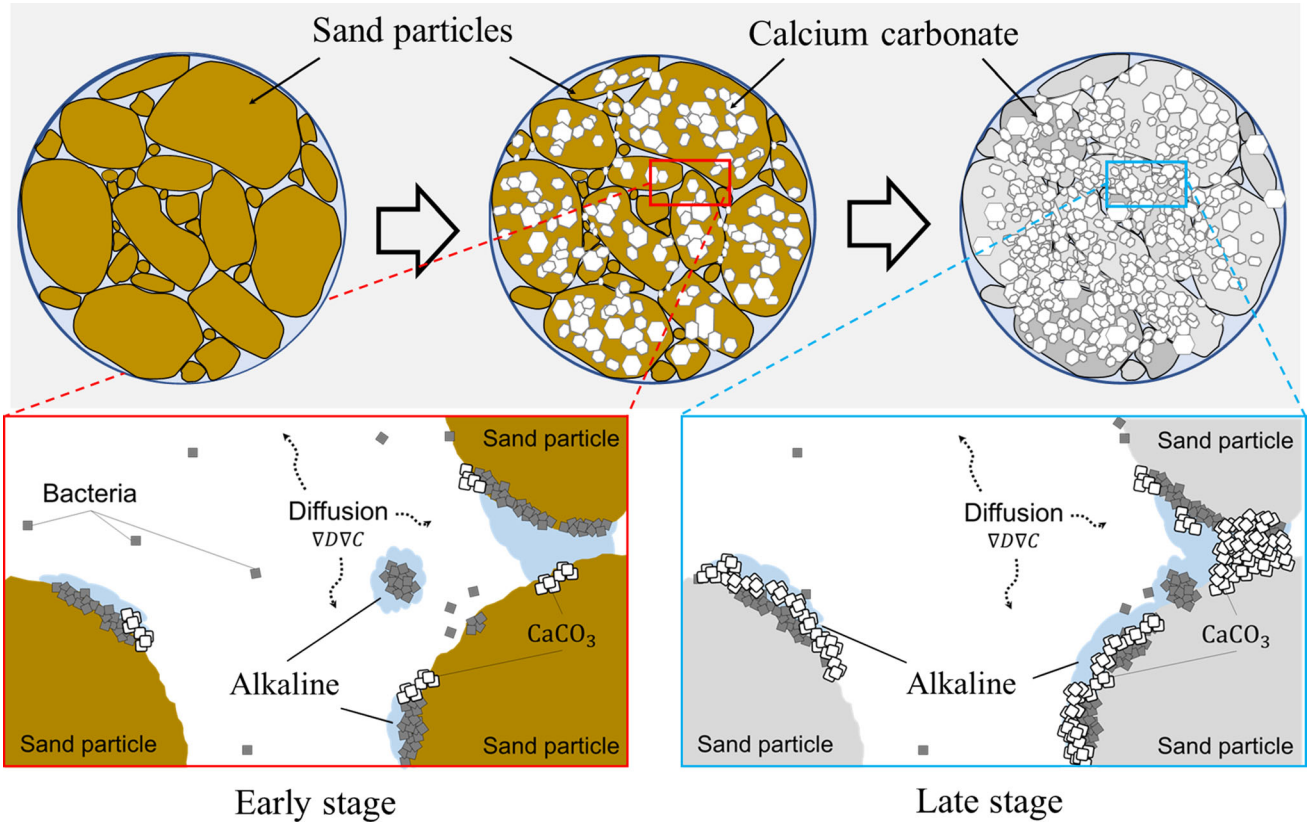

Fig. 1 Ureolytic bacteria induced precipitation of calcium carbonate

strength development of soil micro- and macro-structure. In this regard, we investigated the changes in soil micro-structure and soil mechanical parameters (e.g. elastic modulus) and subsequently conducted the stress analysis. Several multi-scale analysis techniques have been proposed to theoretically relate the micro- and macro-structures [3, 14, 40, 53]. This study utilised finite element method (FEM) based mathematical homogenisation [54] as a bridging technique. This method was suitable because the average values of the material constants of soil micro-structure could be utilised as the mechanical parameters of soil macro-structure.

This study proposed a novel mathematical model considering bacterial colony growth to elucidate the MICP phenomenon. Specifically, the proposed model assessed the relationship between bacterial growth and MICP in three dimensional micro-structures. Additionally, a mathematical homogenisation scheme was applied to investigate the relationship between changes in soil micro-structure due to MICP and the strength development of soil micro- and macro-structure. Furthermore, we constructed coupling models of bacterial growth and MICP. Subsequently, we proposed a technique for transforming a bio-chemical field into a dynamical field in the micro-structure. Finally, the morphological and quantitative results obtained by the numerical simulations were compared with the existing experimental results.

2 Mathematical modelling of micro-scale biosystems

2.1 Growth of ureolytic bacteria

Several studies in the field of mathematical biology have utilised mathematical and numerical models to determine the growth of microbial colonies and elucidate the underlying formation mechanisms [26]. Specifically, a few studies have utilised reaction–diffusion systems in this regard [60]. In particular, reaction–diffusion systems have been utilised to simulate morphological properties such as cell division and colour patterns in living organisms [44, 38]. Notably, bacterial colonies on agar have been shown to indicate specific patterns such as circular, tree-like, and spotted [41]. The mathematical models for growth of bacterial colony were based on the following equation [23, 34]:

$$\frac{\partial u}{\partial t} = D_u \nabla^2 u + (\varepsilon - \mu u)u \tag{1}$$

where t, D_u, u, ε, and μ denote the time, bacterial diffusion coefficient, bacterial concentration, growth rate, and the competition coefficient, respectively. Further, $D_u\nabla^2 u$ represents the diffusion term, while $(\varepsilon - \mu u)u$ indicates the growth term. In this study, Eq. (1) was used as the base equation for calculating the growth of ureolytic bacteria where actual bacterial size is not considered, although the concentration of bacteria is assessed.

Several bacteria, including ureolytic bacteria, exhibit chemotaxis, i.e. movement in response to nutrient gradients [17]. Ureolytic bacteria, such as *Helicobacter pylori*, exhibit chemotaxis to urea—a nutrient utilised in their metabolism [36]. The following mathematical model considered chemotaxis in the estimation of ureolytic bacterial growth.

$$\frac{\partial u}{\partial t} = D_u \nabla^2 u + (\varepsilon - \mu u)u - \gamma \nabla \left(\frac{\nabla c}{(c+1)^2} u \right) \tag{2}$$

where γ is the coefficient of chemotaxis and c is the concentration of chemotaxis substance. In the case of ureolytic bacteria, c is defined as the concentration of urea $(CO(NH_2)_2)$. In this study, Eq. (2) was discretised by the finite difference method.

2.2 Metabolism of ureolytic bacteria

Urea hydrolysis by ureolytic bacteria induces the precipitation of calcium carbonate [61]. Hence, the MICP phenomenon could be represented by urea hydrolysis and calcium carbonate precipitation. The chemical reaction system in this regard was expressed as follows [33]:

$$CO(NH_2)_2 + 2H_2O \underset{k_2}{\overset{k_1}{\rightleftarrows}} CO_3^{2-} + 2NH_4^+ \tag{3}$$

$$Ca^{2+} + CO_3^{2-} \underset{k_4}{\overset{k_3}{\rightleftarrows}} CaCO_3 \tag{4}$$

where Eqs. (3) and (4) describe urea hydrolysis by ureolytic bacteria and the precipitation of calcium carbonate, respectively. This study left the impact of temperature out of account because both that general thermodynamic parameters may not be directly applied to microbial metabolism and that thermodynamic equilibrium parameters may not be introduced directly in non-equilibrium simulations. Thus, in this study, we discuss whether a reaction–diffusion theory approach is effective for the MICP phenomena.

Considering the diffusion and inflow terms in Eqs. (3) and (4), the following mathematical models were constructed based on the reaction–diffusion system:

$$\frac{\partial A}{\partial t} = \nabla(D_A \nabla A) - k_1 A B^2 + k_2 C E^2 + A_{\text{in}} \tag{5}$$

$$\frac{\partial B}{\partial t} = \nabla(D_B \nabla B) - k_1 A B^2 + 2k_2 C E^2 + B_{\text{in}} \tag{6}$$

$$\frac{\partial C}{\partial t} = \nabla(D_C \nabla C) + k_1 A B^2 - k_2 C E^2 - k_3 C F + k_4 P \tag{7}$$

$$\frac{\partial E}{\partial t} = \nabla(D_E \nabla E) + 2k_1 A B^2 - k_2 C E^2 \tag{8}$$

$$\frac{\partial F_{\text{i}}}{\partial t} = \frac{\partial}{\partial x} D_{\text{F}} \frac{\partial F_{\text{i}}}{\partial x} - k_3 C_{\text{i}} F_{\text{i}} + k_4 P + F_{\text{in}} \tag{9}$$

$$\frac{\partial P}{\partial t} = k_3 C_{\text{i}} F_{\text{i}} - k_4 P \tag{10}$$

where A, B, C_{i}, E, F_{i}, and P denote the concentrations of $CO(NH_2)_2$, H_2O, CO_3^{2-}, NH_4^+, Ca^{2+}, and $CaCO_3$, respectively. A_{in}, B_{in}, and F_{in} are the constant inflows of $CO(NH_2)_2$, H_2O, and Ca^{2+}, respectively. k_1 and k_3 in Eqs. (3) and (4) are the positive rate constants of the chemical reaction whereas k_2 and k_4 are the negative rate constants where the reverse reactions were assumed to be very slow in this study. Moreover, D_* is the diffusion coefficient of the related variable (*) which exhibits a random value at micro-scale. These equations were discretised by the finite difference method.

The urease enzyme reaction occurs in ureolytic bacteria, resulting on an increased number of bacteria. This means that if the number of ureolytic bacteria increases, the metabolic response of Eq. (3) would be more active. Therefore, the rate constant k_1 depends on the population of ureolytic bacteria, i.e. k_1 increases as the population of ureolytic bacteria increases and vice versa. In this study, this dependence was obtained based on the concentration of ureolytic bacteria formulated in Eq. (2). Assuming that k_1 at an arbitrary point $\boldsymbol{X}_{\text{i}}$ ($k_1(\boldsymbol{X}_{\text{i}})$) exhibits a linear relationship with the concentration of ureolytic bacteria at that point ($u(\boldsymbol{X}_{\text{i}})$), we obtained the following equation:

$$k_1(\boldsymbol{X}_{\text{i}}) = \frac{k_{1,\max}}{(u_{\max} - u_{\min})} \times u(\boldsymbol{X}_{\text{i}}) - \frac{k_{1,\max} \times u_{\min}}{(u_{\max} - u_{\min})} \tag{11}$$

where $k_{1,\max}$, $u_{\max}$, and $u_{\min}$ are maximum value of k_1, maximum value of u, and minimum value of u, respectively. To date, although this linear relationship is not yet proved, the authors have proposed here as a mathematical model.

3 Homogenisation modelling

3.1 Bridging from micro- to macro-structure

The concentration of calcium carbonate was calculated in a stepwise manner using Eq. (10) to ensure that the inner structure changed step-by-step. Although previous studies have proposed various multi-scale simulation techniques [24], this study considered the mathematical homogenisation method [55] for elucidating the relationship between micro- and macro-structures. This is because the periodic boundary condition for soil micro-structure is almost satisfied if urea and ureolytic bacteria are evenly distributed. Additionally, this method has been widely applied to address various multi-scale problems such as evaluating the properties of rock mass strength, determining fracture patterns, and topological optimisation [32, 46, 51]. Hence, the adoption of this method in this study expands our fields of application.

The homogenised material properties of the soil macro-structure were determined by conducting deformation analyses for a unit cell, i.e. a micro-structure with periodic boundary conditions [39, 43]. The stress in soil micro- and macro-structure was analysed under maintaining their interrelationships. This could be attributed to the bridging of material parameters and deformation at both scales.

If y denotes the coordinate system for a micro-structure, then stress (σ), displacement (u), and strain (ε) in the micro-structure can be described as follows:

$$\frac{d\sigma(y)}{dy} = 0 \text{ in a unit cell} \tag{12}$$

$$\sigma(y) = C\varepsilon(y) \tag{13}$$

$$\varepsilon(y) = \frac{du(y)}{dy} \tag{14}$$

where C is the elastic constant of the micro-scale structure. Further, displacement in the micro-structure was defined as:

$$u(y) = \mathrm{E}(x)y + u^* \tag{15}$$

where x and E denote the coordinate system and the strain in the macro-structure, respectively. u^* is the disturbance displacement determined as:

$$u^* = -\chi \mathrm{E}(x) \tag{16}$$

where χ is the characteristic deformation. The strain in the micro-structure was calculated based on Eqs. (14)–(16) as follows:

$$\varepsilon(y) = \frac{du}{dy} = \mathrm{E}(x) + \frac{du^*}{dx} = \mathrm{E}(x) - \frac{d\chi}{dy}\mathrm{E}(x) \tag{17}$$

The relationship between stress and strain in the macro-structure was governed by the following equation:

$$\Sigma(x) = C^h \mathrm{E}(x) \tag{18}$$

where $\Sigma(x)$ is the stress in the macro-structure, and C^h is the homogenised elastic modulus. Assuming unit strain (1.0) in the macro-structure, Eqs. (17) and (18) were converted as follows:

$$\varepsilon(y) = 1 - \frac{d\chi}{dx} \tag{19}$$

$$\Sigma(x) = C^h \tag{20}$$

Additionally, the relationship between stress and strain was calculated for each scale as follows:

$$\Sigma(x) = \sigma \tag{21}$$

$$\mathrm{E}(y) = \varepsilon \tag{22}$$

where $\langle * \rangle$ represents the average volume of the micro-structure. Therefore, the homogenised elastic modulus was calculated as follows:

$$C^h = \Sigma = \sigma = C\varepsilon = C\left(1 - \frac{d\chi}{dy}\right) \tag{23}$$

In this study, the FEM was employed for discretisation. Subsequently, the element stiffness matrix (K) was calculated as:

$$K = \int_V [B]^T \left[C^h\right][B]dV \tag{24}$$

where V is the volume of the macro-structure and B is the strain–displacement matrix. The estimation of stress distribution in the macro-structure was followed by the calculation of displacement, strain, and stress at arbitrary points in the micro-structure using the following equations:

$$u(y) = \mathrm{E_A}(x)y - \chi \mathrm{E_A}(x) \tag{25}$$

$$\varepsilon(y) = \mathrm{E_A}(x) - \frac{d\chi}{dy}\mathrm{E_A}(x) = \mathrm{E_A}(x)\left(1 - \frac{d\chi}{dy}\right) \tag{26}$$

$$\sigma(y) = C\varepsilon(y) = C\mathrm{E_A}(x)\left(1 - \frac{d\chi}{dy}\right) \tag{27}$$

where A is an arbitrary coordinate in the macro-structure.

3.2 Bridging from micro-scale biosystems to homogenisation systems

In this study, the micro-structure changed in a stepwise manner owing to the MICP phenomenon. Therefore, the concentration of calcium carbonate in the inner structure, including soil particles, was estimated at each time step. Further, we determined its distribution in a unit cell. As indicated in Sect. 2, the finite difference method (FDM) was utilised to calculate the calcium carbonate concentrations of the grid points. Thus, the grid system utilised for MICP simulation was reused as the mesh system for the micro-structure (unit cell) during homogenisation simulation. However, the estimated calcium carbonate concentrations of the grid points should be converted to the material properties of the integral points of the meshes. This is because FEM-based homogenisation analyses require material properties of the integral points of the micro-structure (see Fig. 2.

In this study, calcium carbonate concentrations were interpolated using the shape function of the FEM [66] as indicated by the following equation:

$$P_{ip} = \sum_{j=1}^{8} N_j(x_{ip})P_j \tag{28}$$

where P_{ip} and $N_j(x_{ip})$ denote the concentration of calcium carbonate and the value of the shape function at an integral point (ip), respectively. Notably, this study utilised 27 integral points per mesh. Further, j is the grid number of the constructing structure.

Martinez et al. [31] experimentally elucidated the relationship between calcium carbonate concentration and shear wave velocity (V_s) as denoted by Eq. (29).

$$V_s = 1.053P + 157.895 \tag{29}$$

Shear wave velocities were converted to shear modulus values (G) using Eq. (30):

$$G = \rho \times V_s^2 \tag{30}$$

where $\rho(= 2.71\ \mathrm{g/cm^3})$ is the density of calcium carbonate.

The bridging scheme described above allowed seamless multi-scale simulation of ureolytic bacterial growth, MICP, elastic micro-structure, and elastic macro-structure. A flowchart of the proposed technique is presented in Fig. 3.

4 Numerical examples

4.1 Model and boundary conditions

Figure 4 presents the initial structure models for the simulation of microbial growth and MICP. Further, these models were used as unit cells during homogenisation simulation. The size of each model was 1mm × 1mm × 1mm. Further, each axial direction (x, y,

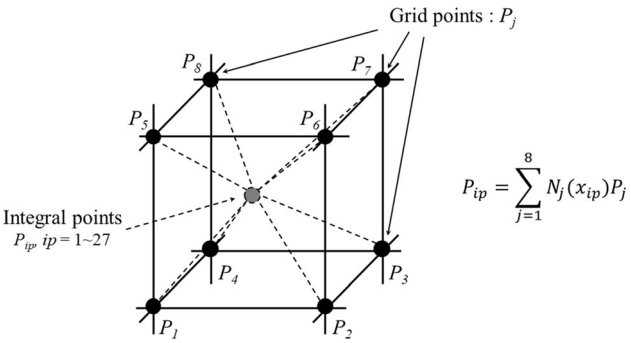

Fig. 2 Interpolation of calcium carbonate concentration of an integral point based on the grid point values

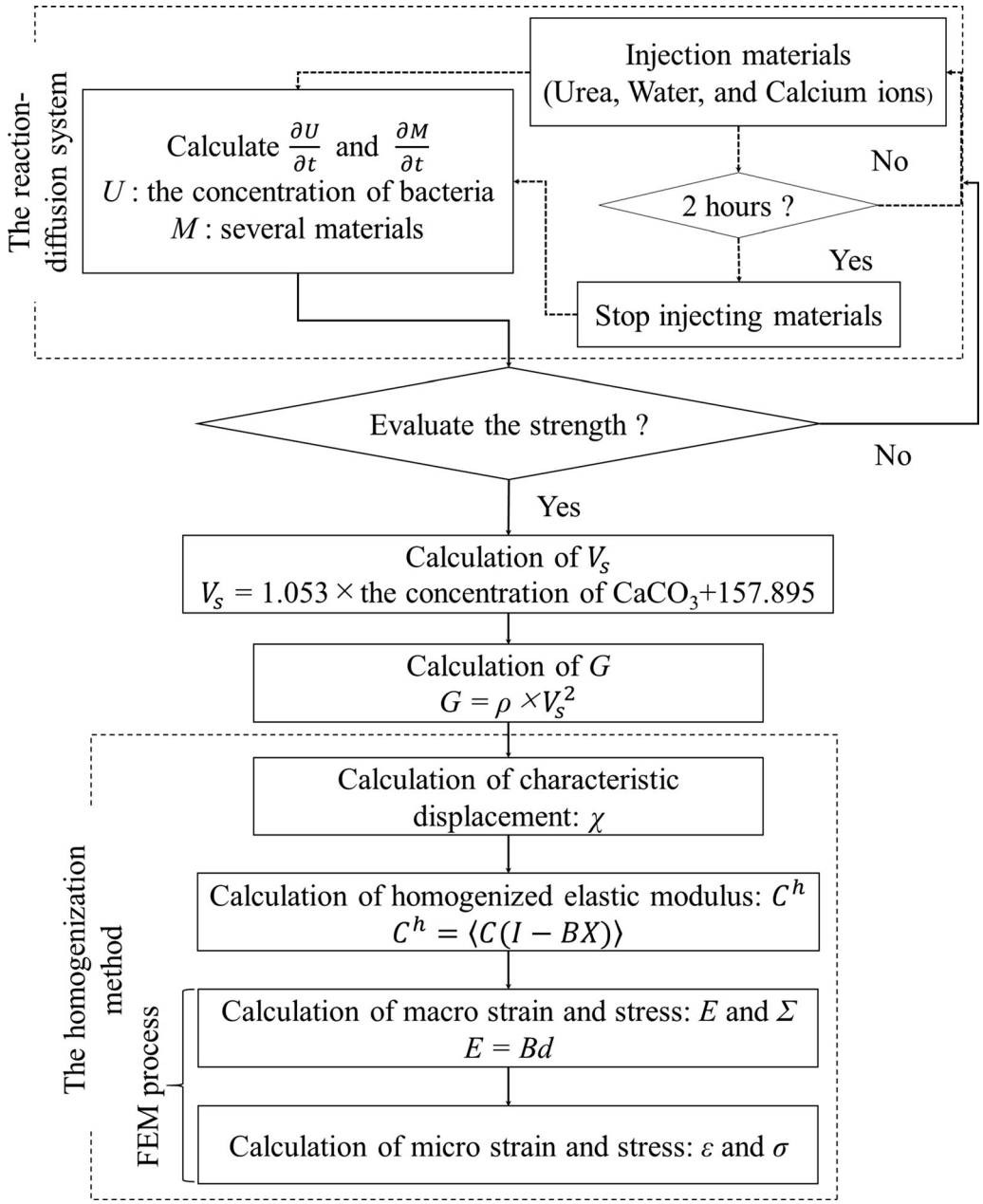

Fig. 3 Flowchart of the proposed simulation

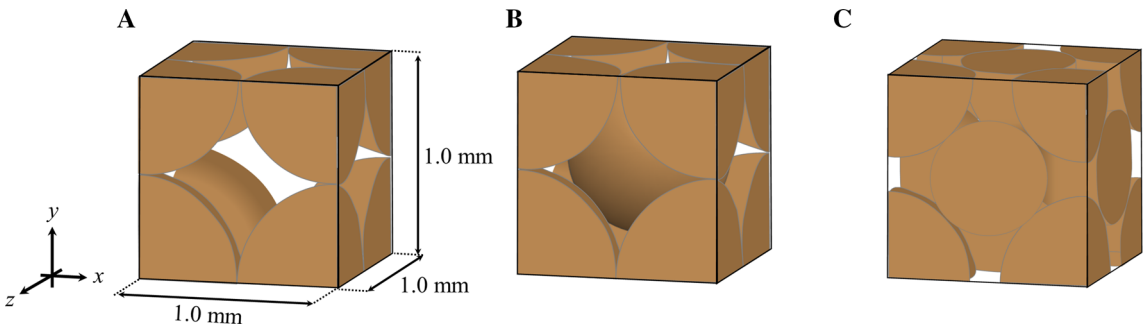

Fig. 4 Initial structure models of sand particles in the MICP system: **a** Model1 (coarse model); **b** Model 2 (medium dense model), **c** Model 3 (dense model)

and z) was divided by 64 (number of grid points: 274,625). The arrangement of sand particles may have a significant influence on the precipitation pattern because the target of this study is a micro-scale area of sand particle size. Therefore, as shown in Fig. 4, three models arranged several spherical sand particles in the cube were prepared. In model 1, eight spherical sand particles (radius: 0.5 mm) were placed at each vertex Fig. 4a. In model 2, eight spherical sand particles (radius: 0.5 mm) were placed at each vertex and one particle (radius: $(\sqrt{3}-1)/2$ mm) was placed at the centre of the cube Fig. 4b. In model 3, 14 spherical sand particles (radius: $\sqrt{2}/4$ mm) were placed at each vertex and at the centre of the faces Fig. 4c.

The simulation was characterised by a time increment (Δt) of 0.001 h. Further, the diffusion coefficients were randomly selected. Specifically, the diffusion coefficients of materials (D_A, D_B, D_C, D_E, D_F) were set to $6.08 \times 10^{-3} \sim 2.56 \times 10^{-2}$ mm^2/h [4] because the diffusion of substances and ions in general solution were assumed. With respect to the diffusion coefficient of ureolytic bacteria (D_u) was set to 1.00×10^{-4} mm^2/h because the authors assumed that the movement of bacteria largely depends on chemotaxis in Eq. (2), and the effect of diffusion themselves is smaller than that of other substances and ions. In contrast, to date, no studies have been conducted to accurately know the values of the growth rate (ε), competition coefficient (μ), and the coefficient of chemotaxis (γ) in ureolytic bacteria. Therefore, these values were determined based on existing studies on *Helicobacter pylori* and *Escherichia coli*, etc. [5, 19, 49] in this study. That is, the growth rate, competition coefficient, and the coefficient of chemotaxis were set to 0.4 /h, 2.0×10^{-3} cells/h, and 2.5 mm^2/h, respectively.

The k_1 is determined by Eq. (11) that is a linear model to express the relationship between reaction rate and bacterial concentration. In contrast, the negative rate constants k_2 and k_4 were set as 1.0×10^{-4} and 0.1 μmol/mm^2/h, respectively, because the reverse reactions were assumed to be very slow in this study. In contrast, the value of k_3 was set to 1.0×10^6 μmol/mm^2/h based on the existing experiment on natural calcite precipitation [8]. Additionally, the external injections of A_{in} in Eq. (5), B_{in} in Eq. (6), and F_{in} in Eq. (9) were set to 1.45, 4.37×10^{-1}, and $4.29 \times 10^{-1} \mu$mol/mm^3, respectively, in the unit cells. These values are identical in the experiment of Case 1A [31] for comparing the results of the simulation with those of the experiment. Also, the initial value of bacterial concentration was set to 4.0×10^8 cells/mm^3 [31]. Additionally, the experiment by Martinez et al. [31] indicated that the concentration of ureolytic bacteria was lower than the initial injection. Converting the initial injection to the amount on a grid point used in this study denotes 3.0×10^3 cells/mm^3. Based on their finding, the authors hypothesised that the concentration of ureolytic bacteria in the container would not be more than double the initial injection, thus the u_{max} were u_{min} in Eq. (11) were defined as 7.0×10^3 and 0.0 cells/mm^3, respectively, where the values were set on the grid, point by point. The parameters setting shows in Table 1.

In contrast, as indicated in Fig. 5, a cuboid structure (50mm × 100mm × 50mm) represented the macro-structure. Each axial direction (X, Y, and Z) of this structure were divided by 20, 40, and 20., respectively. A compression force of 1.0 N was applied to each nodal point of the top surface of the structure as the simulation load condition. Further, nodal displacement on the bottom surface was completely constrained at coordinates (X, Y, Z) = (0, 0, 0). Moreover, displacement at the other nodes of the bottom surface was constrained in the Y direction.

4.2 Simulation results

Figure 6 presents the temporal variation in ureolytic bacterial concentration as determined by Eq. (2). All models indicated an exponential decrease in the bacterial concentration. Further, the maximum concentrations obtained by models 1, 2, and 3 were 1.7×10^8, 1.3×10^8, and 9 .3 × 10^7 cells/mm^3, respectively, during the early elapsed time (∼ 0.5 h). Figure 7 present the temporal variation in the

Table 1 Parameters setting

Parameters	Values	Units	References
D_u	1.00×10^{-4}	mm^2/h	[4]
D_A, D_B, D_C, D_E,D_F	$6.08 \times 10^{-3} \sim 2.56 \times 10^{-2}$		
A_{in}	1.45	μ mol/mm^3	[31]
B_{in}	4.37×10^{-1}		
F_{in}	4.29×10^{-1}		
u_i (Initial concentration)	4.0×10^8(Total) 3 .0 × 10^3 (Each grid)	cells/mm^3	
u_{max}	7.0×10^3		
u_{min}	0.0		
ε	0.4	h^{-1}	[19]
μ	2.0×10^{-3}	cells/h	[5]
μ	2.5	mm^2/h	[49]
k_1	Calculated by Eq. (11)	μ mol/mm^2/h	[8]
k_2	1.0×10^{-4}		
k_3	1.0×10^6		
k_4	0.1		

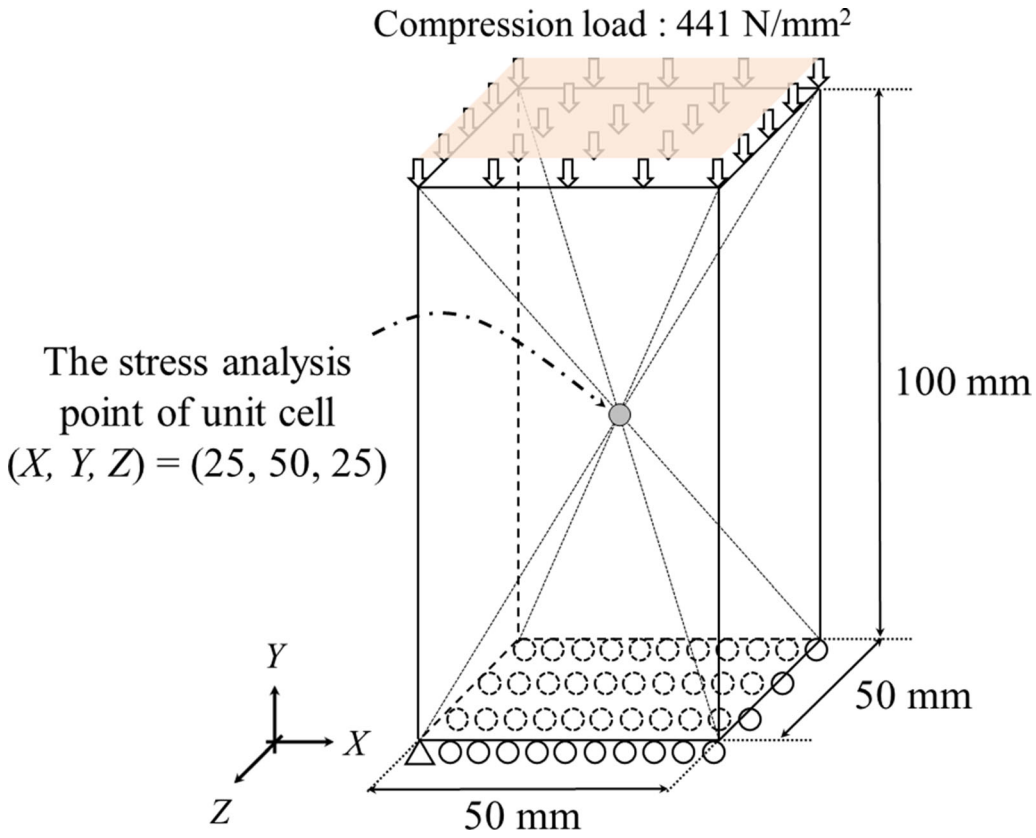

Fig. 5 Macro-structural model and boundary conditions of the homogenisation system

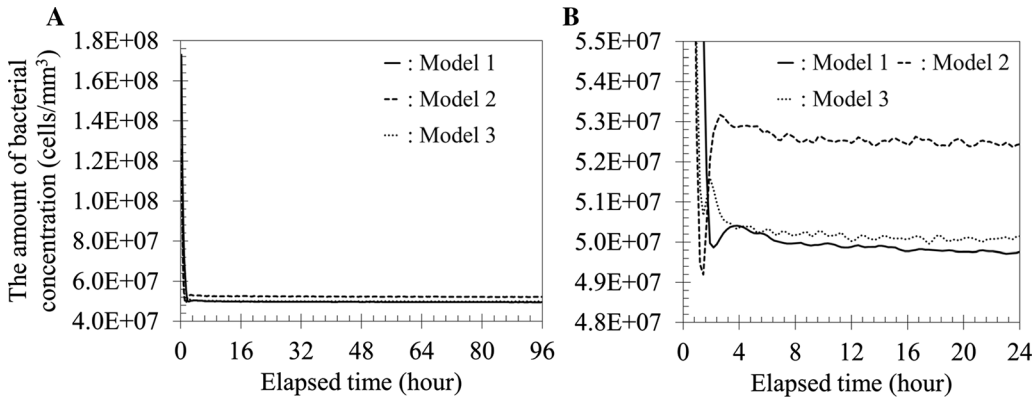

Fig. 6 Temporal variation in the concentration of ureolytic bacteria: **a** Full-time scale (0 to 96 h), **b** Zooming of 0 to 24 h in (**a**)

distribution of bacterial colonies for each model. The colour contour in Fig. 7 indicates the bacterial concentration where the maximum one is displayed in yellow and the minimum one was in blue. The results indicated that ureolytic bacteria formed spot-like colonies in the pores and on the surface of sand particles. Specifically, as indicated in Figs. 7b and 7c, the bacteria inhabited pores and the surface of sand particle during the initial stage and were concentrated in the gaps between the sand particles with increasing elapsed time.

The temporal variation in the concentrations of urea, calcium ions, carbonate ions, and water represented by Eqs.(3) and (4) (excluding calcium carbonate) as simulated by the different structural models is presented in Fig. 8. Although the models indicated different absolute concentrations of the substances, they exhibited similar temporal variations. Figure 9 presents the temporal variation in the total concentration of calcium carbonate. It should be noted that the experimental results by Martinez et al. [31] have been plotted as a reference value. All models indicated

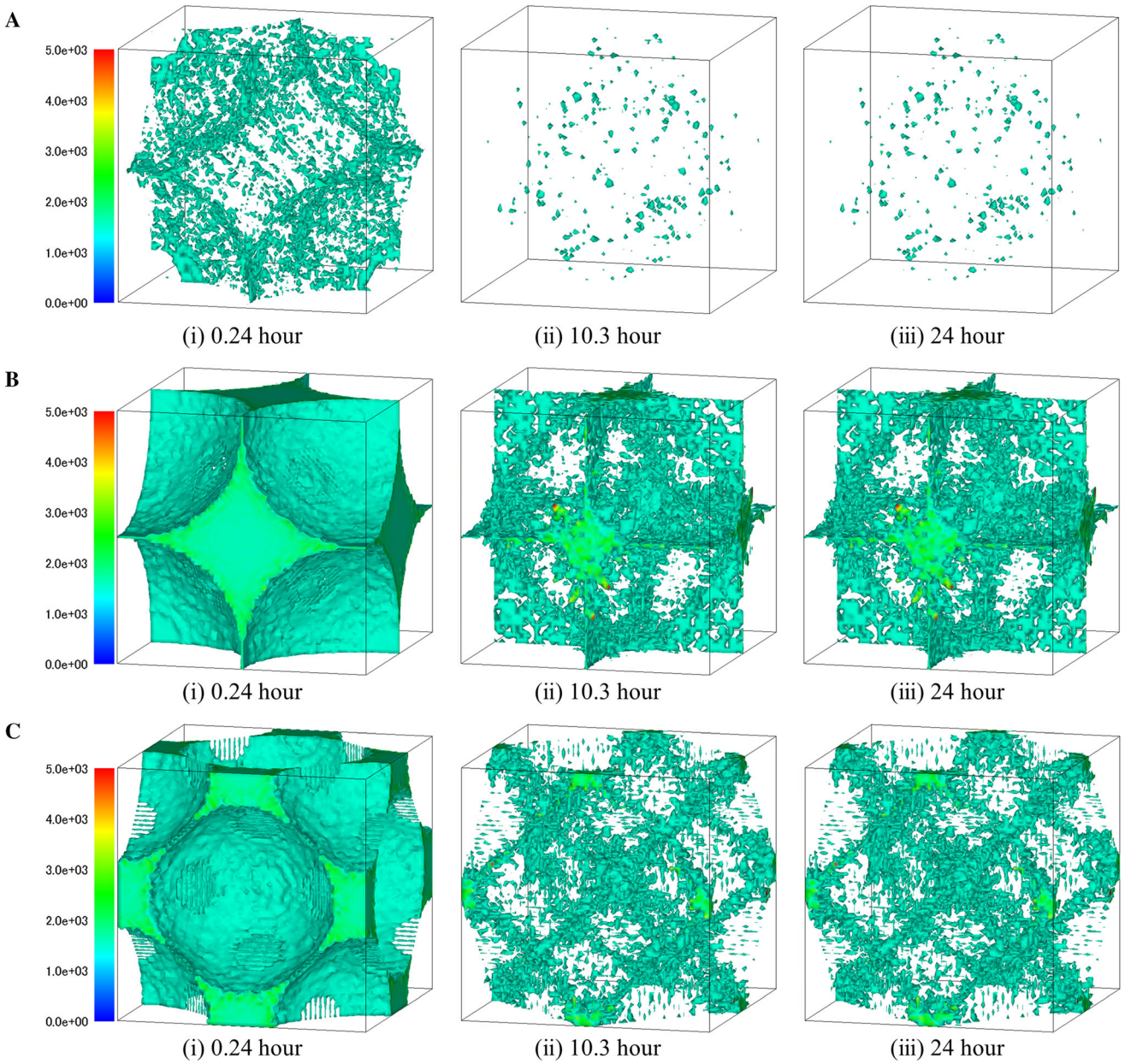

Fig. 7 Temporal variations in the distribution of bacterial colonies in the cases of **a** Model 1, **b** Model 2, and **c** Model 3

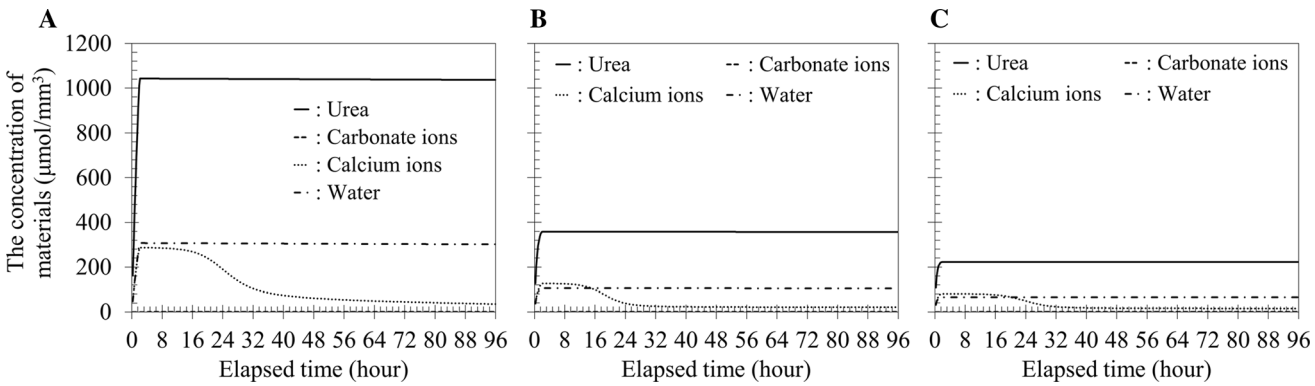

Fig. 8 Temporal variation in concentrations (excluding calcium carbonate) in the cases of **a** Models 1, **b** Model 2, and **c** Model 3

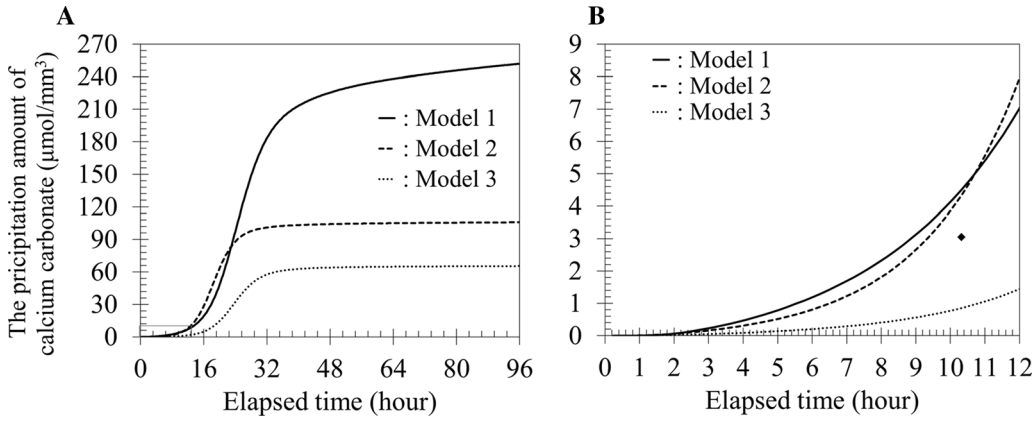

Fig. 9 Temporal variation in calcium carbonate concentration in models 1, 2, and 3: **a** Full-time scale (0 to 96 h), **b** Zooming of 0 to 12 h in (**a**)

increased calcium carbonate precipitation at the initial stage. Further, models 1, 2, and 3 converged to a specific value after approximately 48, 36, and 36 h of elapsed time, respectively. Moreover, the values obtained from models 1 and 2 Fig. 9b were in good agreement with those reported by Martinez et al. [31].

Figure 10 indicates the temporal variation in the distribution of precipitated calcium carbonate for each model. The results indicated that sand particles combined with each other over time owing to the precipitated calcium carbonate. Notably, as indicated in model 1 Fig. 10a, a few cores of calcium carbonate precipitated at approximately 10.3 h. Subsequently, calcium carbonate developed around these cores and on the surface of sand particles. In contrast, no cores were observed in models 2 and 3 Figs. 10b and c, respectively). However, calcium carbonate precipitated and developed around and on the surface of sand particles.

Figure 11 indicates the equivalent faces of normal stress calculated by the homogenisation system considering microbially induced calcium carbonate precipitation. Although the different skeleton structures of the models resulted in different values and distributions, the concentration of normal stress relaxed over time in all models.

5 Discussion

Figures 6 and 7 indicate that the impact of skeleton structure on the growth rate of ureolytic bacteria was relatively small. Further, the bacterial colonies concentrated around and on the surface of sand particles over time. Previous laboratory studies have reported that some bacteria can exhibit several colony patterns [41, 34]. In particular, bacterial colonies have been shown to indicate spot-like patterns during chemotaxis [45]. Additionally, bacterial growth can be modelled by logistic equations [23]. Figure 6 indicates that the variation in bacterial concentration stabilised after ∼ 1.5–2.0 h, which is similar to a logistic curve. Further, the simulation results indicated spot-like colony patterns Fig. 7, thus suggesting good agreement with previous experimental studies [12, 34]. Notably, the spot-like distribution of ureolytic bacteria induced spot-like precipitation of calcium carbonate Fig. 10a. Hence, the reaction–diffusion system-based model considering chemotaxis could quantitatively estimate the ureolytic bacterial growth.

Let us consider the temporal variation of urea, calcium ions, carbonate ions, water, and calcium carbonate. Although the same amount of urea was injected for a duration of two hours following Martinez et al. [31], models 2 and 3 indicated lower absolute concentrations of substances than model 1 Fig. 8. Model 1 was characterised by the largest pore volume; therefore, it could store larger substances in contrast to models 2 and 3. Specifically, the pore volumes of models 1, 2, and 3 were 0.48, 0.27, and 0.26 mm^3, respectively. Figure 12 presents the temporal variation in the concentrations of discharged substances for each model. These results suggest that the substance concentrations simulated by the models converged similarly over time. Further, the concentrations predicted by model 1 were half of those simulated by models 2 and 3. In particular, most of the substances injected into model 1 remained inside the pore. However, the substances were discharged outside the region in models 2 and 3. Therefore, the differences in the substance concentrations simulated by the models could be attributed to the discharge of substances (including urea) from the analytical to the external area.

Previous experimental studies have reported that calcium carbonate precipitates on the surface of and/or between sand particles in sandy soils [9, 50]. As indicated in Fig. 10, calcium carbonate precipitated both on the surface of and between sand particles in the proposed models. Subsequently, calcium carbonate grew into the

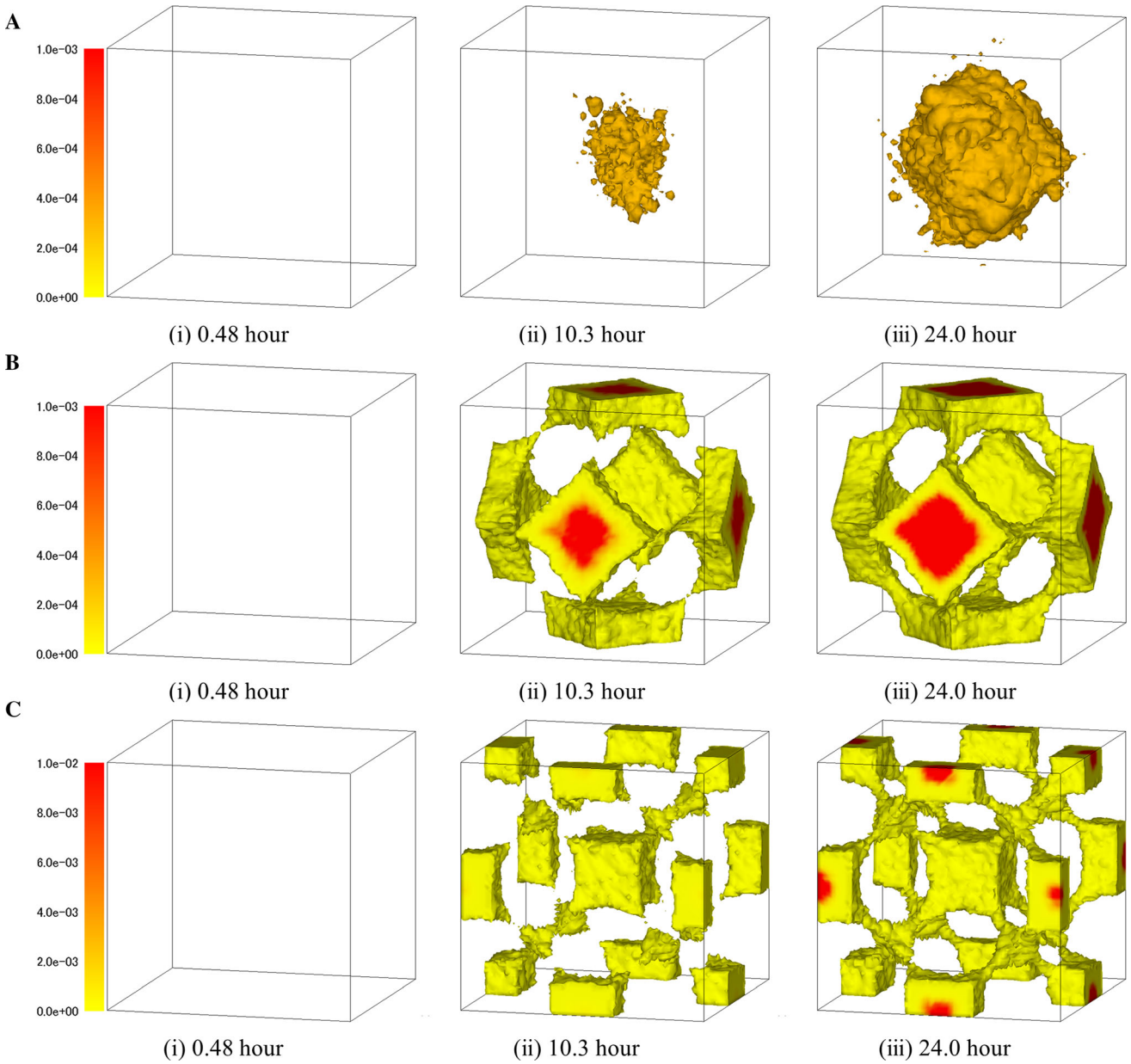

Fig. 10 Temporal variations in precipitated calcium carbonate in the cases of **a** Model 1, **b** Model 2, and **c** Model 3

pore region with elapsed time. Figure 13 presents the quantitative temporal distributions of calcium carbonate concentrations on the x-lines of the *x*–*y* surface for the three models. The *z* value for all models was 0.343 mm, while the y values were 0.312, 0.5, and 0.73 mm. These results suggest a gradual precipitation of calcium carbonate. The zero values (e.g. in Fig. 13a(i)) indicate sandy particle areas with no calcium carbonate precipitation. Subsequently, calcium carbonate grew around the sandy particles to combine them, thus resulting in the formation of a new skeleton structure. As indicated in Fig. 7, the precipitation area of calcium carbonate was in good agreement with the distribution of bacterial colonies. The clumpy patterns Fig. 10a observed in this study have also been reported in previous studies [7, 12, 13]. Therefore, the proposed model considering bacterial growth could assess MICP both quantitatively and morphologically.

Previous studies evaluating the relationship between MICP and material strength have concluded that bio-mediated cementation can enhance strength and reduce deformation of sand [22, 37]. Furthermore, the shear wave velocity of materials has been shown to increase with progressing MICP [12, 13]. The simulation results Fig. 11 indicated that the normal stress concentrations relaxed over time as the pores were gradually filled by calcium carbonate. Figure 14 present the distributions of normal stress

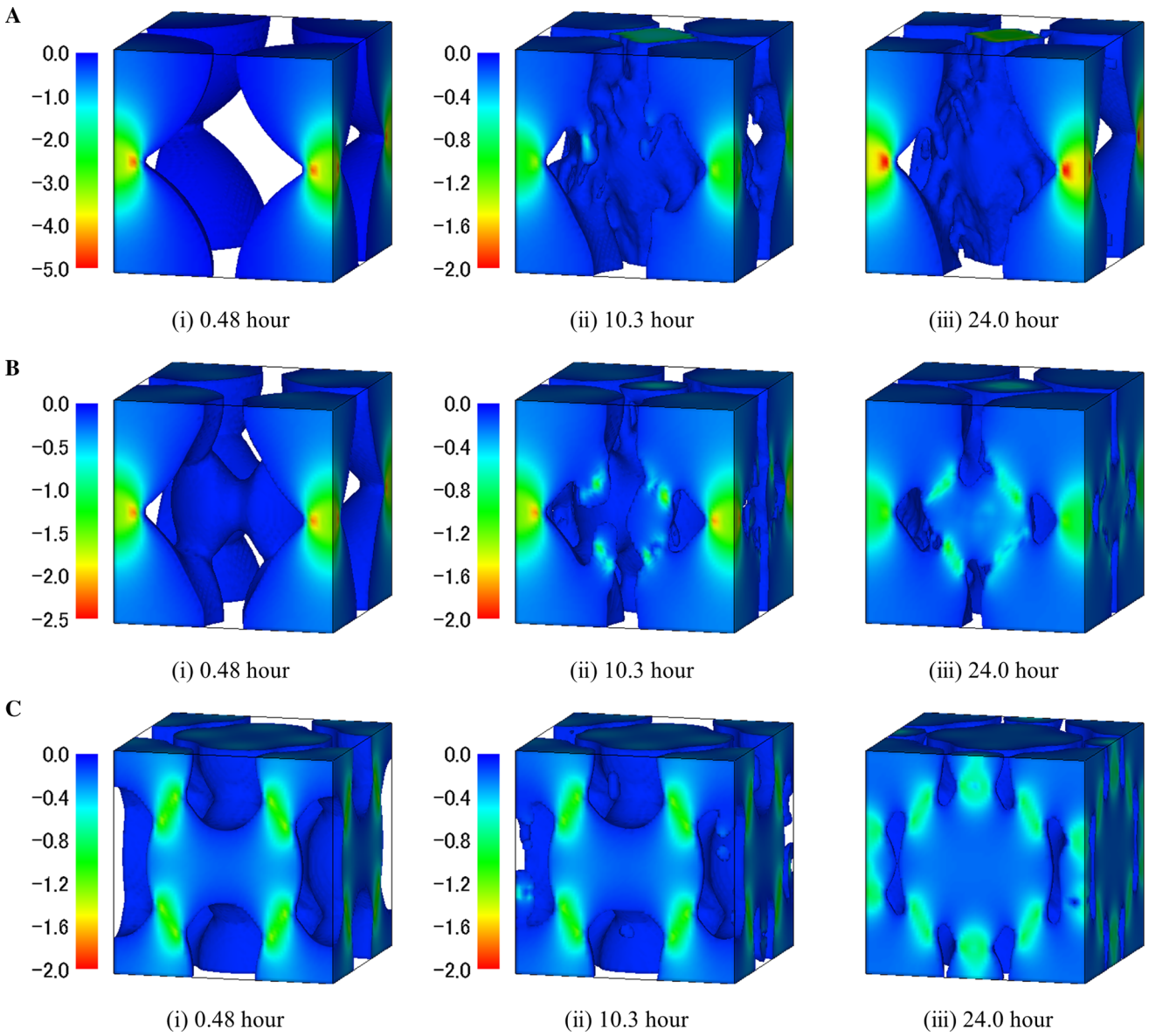

Fig. 11 The equivalent faces of normal stress (model 1; unit: N/mm^2) in the cases of **a** Model 1, **b** Model 2, and **c** Model 3

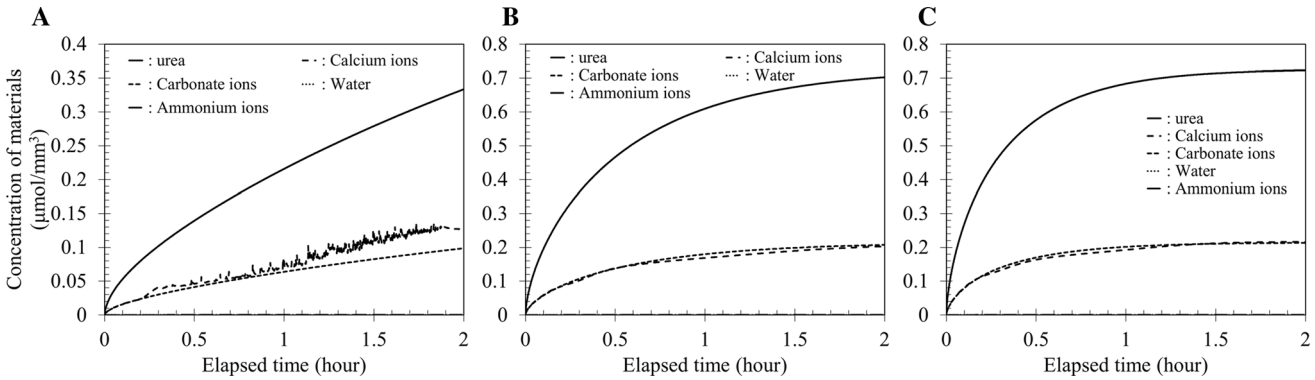

Fig. 12 Temporal variation in the concentrations of discharged substances in the cases of **a** Model 1, **b** Model 2, and **c** Model 3

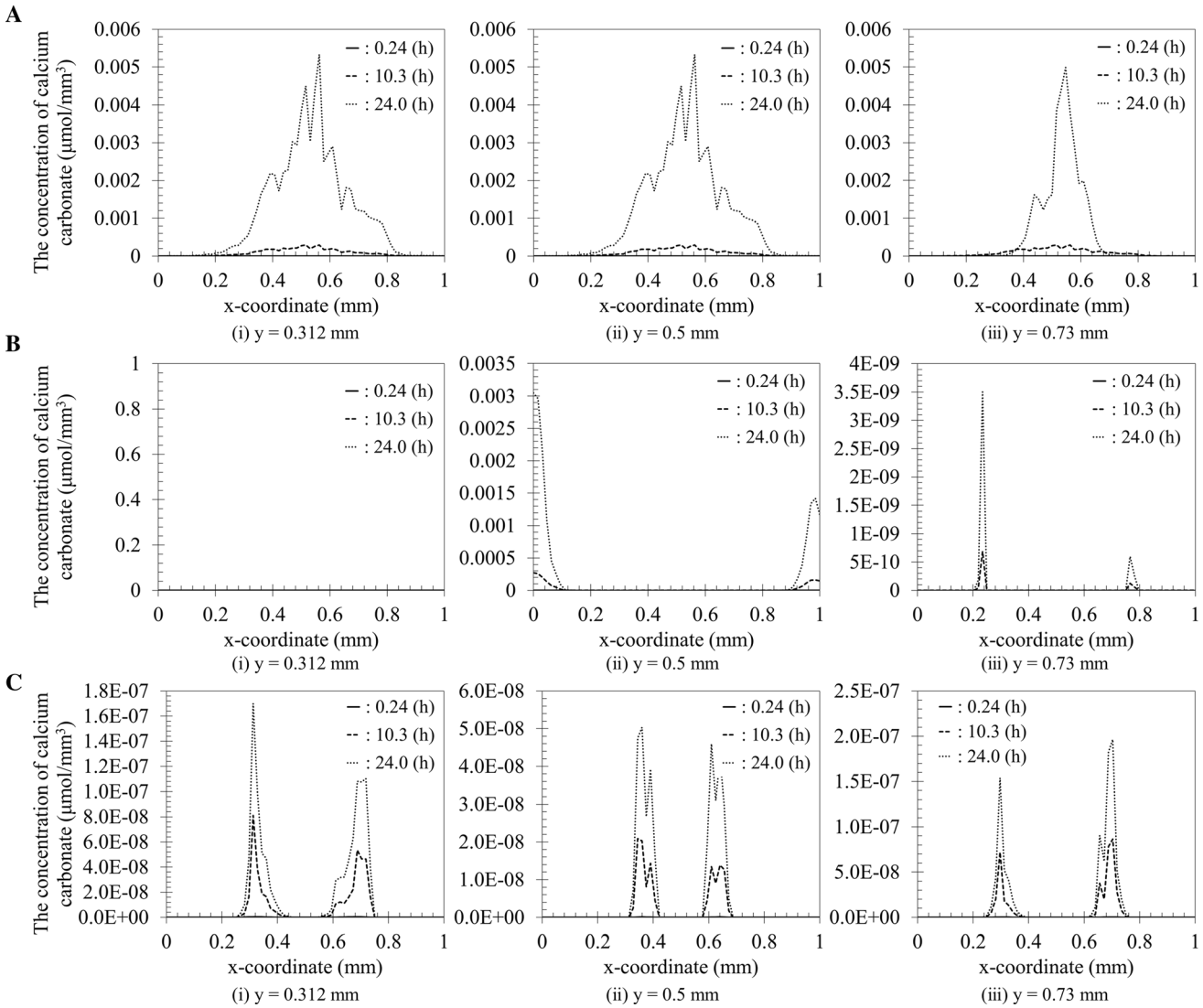

Fig. 13 Distribution of calcium carbonate on the *x*-lines of the *x*–*y* surface; $z = 0.343$ mm in the cases of **a** Model 1, **b** Model 2, and **c** Model 3

on the x-lines of the *x*–*y* surface ($z = 0.352$ mm and $y = 0.298$, 0.501, and 0.751 mm in all models). The results suggest that although the stress concentration observed by initial stage, it eventually relaxed across the entire area. Moreover, the increased stability and strength of soil was predominantly attributed to reduced stress concentrations at the connection points between soil particles. Therefore, a new skeleton structure—characterised by soil particles and calcium carbonate-filled pores—provided support against external forces to consequently relax the stress concentration. For instance, a compression force of 441 N was loaded on the top surface (surface area: 2500 mm^2) of a cuboid structure Fig. 5. The normal stress of the structure without pores was approximately 0.18 N/mm^2. As indicated in Figs. 11 and 14, the normal stress of the structure was eventually homogenized to 0.18 N/mm^2.

As discussed above, we may evaluate the effect of structural changes caused by micro-scale MICP phenomena on their macro-scale deformation characteristics using the homogenisation system. Therefore, the proposed approach would assist in assessing some mechanical features of actual MICP soil strengthening.

6 Conclusions

This study developed a numerical mathematical model considering bacterial growth and chemical reactions to elucidate the strength development of soils by MICP. Our interpretations of the simulation results are summarised as follows:

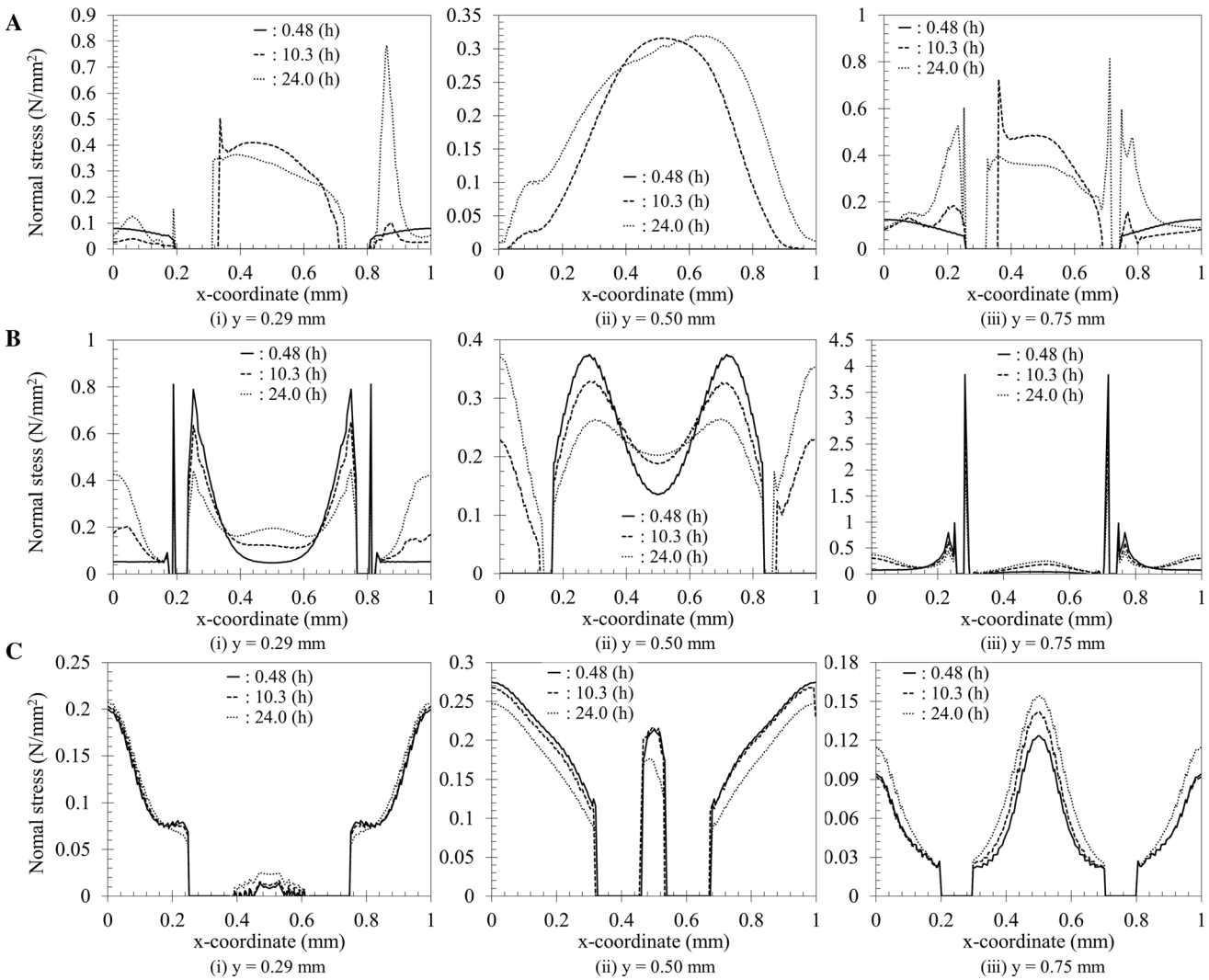

Fig. 14 Distribution of normal stress on the *x*-lines of the *x*–*y* surface; $z = 0.352$ mm in the cases of **a** Model 1, **b** Model 2, and **c** Model 3

(1) The proposed MICP simulation scheme considering microbial growth elucidated the spatio-temporal patterns of both calcium carbonate and bacterial precipitation. Further, we observed some active and inactive bond structures in the pores and on the surface of sand particles in the proposed simulation.

(2) The simulated concentration of calcium carbonate (0.85–4.5 μmol/mm^3 at 10.3 h) was almost consistent with experimental results (3.05 μmol/mm^3), and we could obtain some bonding morphologies in the proposed simulations Fig. 10. The proposed model and approach, based on reaction–diffusion theory, are therefore effective for MICP phenomena.

(3) A bridging scheme based on the homogenisation method was proposed to couple MICP simulation (based on a reaction–diffusion system) and stress analysis (based on a homogenisation system).

(4) The stress analyses indicated that the increased stability and strength of soil could be attributed to the formation of a new skeleton structure comprising soil particles and calcium carbonate-filled pores. Additionally, the filling process relaxed the stress concentrations.

The proposed scheme elucidated the relationship between bacterial growth and MICP. Further, the relationship between MICP in the micro-structure and soil mechanical behaviour in the macro-structure was also investigated. However, we could not achieve to assess the uncertainty of microorganisms, and more comparative studies with experimental data are necessary. Moreover, the crystalline structures of calcium carbonate, amorphous, calcite, aragonite, and vaterite cannot be distinguished in the proposed model because any metastable transition of calcium carbonates cannot be considered in this model.

The authors would like to try this as the upcoming work to address these issues.

Acknowledgement The authors acknowledge the helpful comments and discussions by Prof. Yasuyuki Kanda, Prof. Takashi Ito, and Dr. Kosaburo Hirose of the University of the Ryukyus. This work was supported by the University of the Ryukyus Strategic Research Grant (17SP01301).

References

1. Akiyama M, Kawasaki S (2019) Biogeochemical simulation of microbially induced calcite precipitation with Pararhodobacter sp. strain SO1. Acta Geotech 14(3):685–696
2. Altermann W, Kazmierczak J, Oren A, Wright DT (2006) Cyanobacterial calcification and its rock-building potential during 3.5 billion years of Earth history. Geobiology 4(3):147–166
3. Bendøse MP, Kikuchi N (1988) Generating optimal topologies in structural design using a homogenization method
4. Boving TB, Grathwohl P (2001) Tracer diffusion coefficients in sedimentary rocks: correlation to porosity and hydraulic conductivity. J Contam Hydrol 53(1–2):85–100
5. Budrene EO, Breg HC (1995) Dynamics of formation of symmetrical patterns by chemotactic bacteria. Nature 376(6535):49–53
6. Cheng L, Shahin MA, Chu J (2019) Soil bio-cementation using a new one-phase low-pH injection method. Acta Geotech 14(3):615–626
7. Choi SG, Chang I, Lee M, Lee JH, Han JT, Kwon TH (2020) Review on geotechnical engineering properties of sands treated by microbially induced calcium carbonate precipitation (MICP) and biopolymers. Constr Build Mater 246:118415
8. Chou LEI, Garrels RM, Wollast R (1989) Comparative study of the kinetics and mechanisms of dissolution of carbonate minerals. Chem Geol 78(3–4):269–282
9. Dadda A, Geindreau C, Emeriault F, Du Roscoat SR, Garandet A, Sapin L, Filet AE (2017) Characterization of microstructural and physical properties changes in biocemented sand using 3D x-ray microtomography. Acta Geotech 12(5):955–970
10. Danjo T, Kawasaki S (2016) Microbially induced sand cementation method using Pararhodobacter sp. strain SO1, inspired by beachrock formation mechanism. Mater Trans 57(3):428–437
11. De Muynck W, De Belie N, Verstraete W (2010) Microbial carbonate precipitation in construction materials: a review. Ecol Eng 36(2):118–136
12. DeJong JT, Fritzges MB, Nüsslein K (2006) Microbially induced cementation to control sand response to undrained shear. J Geotech Geoenviron 132(11):1381–1392
13. DeJong JT, Mortensen BM, Martinez BC, Nelson DC (2010) Bio-mediated soil improvement. Ecol Eng 36(2):197–210
14. Díaaz AR, Kikuchi N (1992) Solutions to shape and topology eigenvalue optimization problems using a homogenization method. Int J Numer Meth Eng 35(7):1487–1502
15. Dickson JS, Koohmaraie M (1989) Cell surface charge characteristics and their relationship to bacterial attachment to meat surfaces. Appl Environ Microbiol 55(4):832–836
16. Dupraz C, Reid RP, Braissant O, Decho AW, Norman RS, Visscher PT (2009) Processes of carbonate precipitation in modern microbial mats. Earth-Sci Rev 96(3):141–162
17. El-Sayed AMA, Rida SZ, Arafa AAM (2009) On the solutions of time-fractional bacterial chemotaxis in a diffusion gradient chamber. Int J Nonlinear Sci 7(4):485–492
18. Fein JB (2006) Thermodynamic modeling of metal adsorption onto bacterial cell walls: current challenges. Adv Agron 90:179–202
19. Ford RM, Lauffenburger DA (1991) Analysis of chemotactic bacterial distributions in population migration assays using a mathematical model applicable to steep or shallow attractant gradients. Bull Math Biol 53(5):721–749
20. Fujita Y, Ferris FG, Lawson RD, Colwell FS, Smith RW (2000) Subscribed content calcium carbonate precipitation by ureolytic subsurface bacteria. Geomicrobiol J 17(4):305–318
21. Gallagher PM, Pamuk A, Abdoun T (2007) Stabilization of liquefiable soils using colloidal silica grout. J Mater Civil Eng 19(1):33–40
22. Gao Y, Hang L, He J, Chu J (2019) Mechanical behaviour of biocemented sands at various treatment levels and relative densities. Acta Geotech 14(3):697–707
23. Golding I, Kozlovsky Y, Cohen I, Ben-Jacob E (1998) Studies of bacterial branching growth using reaction–diffusion models for colonial development. Phys A 260(3–4):510–554
24. Guedes J, Kikuchi N (1990) Preprocessing and postprocessing for materials based on the homogenization method with adaptive finite element methods. Comput Methods Appl Mech Eng 83(2):143–198
25. Hammes F, Verstraete W (2002) Key roles of pH and calcium metabolism in microbial carbonate precipitation. Rev Environ Sci Biotechnol 1(1):3–7
26. Ito K, Mizuno Y (2009) Numerical morphological analysis of fungal growth based on a reaction-diffusion model. Biocontrol sci 14(1):21–30
27. Ivanov V, Chu J (2008) Applications of microorganisms to geotechnical engineering for bioclogging and biocementation of soil in situ. Rev Environ Sci Biotechnol 7(2):139–153
28. Kazemian S, Huat BB (2010) Assessment of stabilization methods for soft soils by admixtures. In 2010 Int Conf Sci Soc Res (CSSR 2010), IEEE, pp 118–121
29. Krajewska B (2018) Urease-aided calcium carbonate mineralization for engineering applications: a review. J Adv Res 13:59–67
30. Liu B, Zhu C, Tang CS, Xie YH, Yin LY, Cheng Q, Shi B (2020) Bio-remediation of desiccation cracking in clayey soils through microbially induced calcite precipitation (MICP). Eng Geol 264:105389
31. Martinez BC, DeJong JT, Ginn TR, Montoya BM, Barkouki TH, Hunt C, Tanyu B, Major D (2013) Experimental optimization of microbial-induced carbonate precipitation for soil improvement. J Geotech Geoenviron 139(4):587–598
32. Maghous S, de Buhan P, Bekaert A (1998) Failure design of jointed rock structures by means of a homogenization approach. Mechanics of Cohesive—frictional Materials. Int J Exp Model Comp Mater Struct 3(3):207–228
33. Matsubara H, Yamada T (2020) Mathematical modelling and simulation of microbial carbonate precipitation: the urea hydrolysis reaction. Acta Geotech 15(1):29–38
34. Matsushita M, Wakita J, Itoh H, Watanabe K, Arai T, Matsuyama T, Sakaguchi H, Mimura M (1999) Formation of colony patterns by a bacterial cell population. Phys A 274(1–2):190–199
35. Matsushita M, Hiramatsu F, Kobayashi N, Ozawa T, Yamazaki Y, Matsuyama T (2004) Colony formation in bacteria: experiments and modeling. Biofilms 1(4):305
36. Mizote T, Yoshiyama H, Nakazawa T (1997) Urease-independent chemotactic responses of Helicobacter pylori to urea, urease inhibitors, and sodium bicarbonate. Infect Immun 65(4):1519–1521
37. Montoya BM, DeJong JT, Boulanger RW (2013) Dynamic response of liquefiable sand improved by microbial-induced calcite precipitation. Géotechnique 63(4):302

38. Murray JD (2001) Mathematical biology II: spatial models and biomedical applications. Springer, New York
39. Nishi S, Terada K, Kato J, Nishiwaki S, Izui K (2018) Two-scale topology optimization for composite plates with in-plane periodicity. Int J Numer Meth Eng 113(8):1164–1188
40. Nishiwaki S, Frecker MI, Min S, Kikuchi N (1998) Topology optimization of compliant mechanisms using the homogenization method. Int J Numer Meth Eng 42(3):535–559
41. Ohgiwari M, Matsushita M, Matsuyama T (1992) Morphological changes in growth phenomena of bacterial colony patterns. J Phys Soc Jpn 61(3):816–822
42. Oshiro H, Matsubara H (2018) Carbonate precipitation through photoautotrophic microorganisms at the Giza cliff in Okinawa. Japan Environ Earth Sci 77(16):591
43. Oskay C, Fish J (2007) Eigendeformation-based reduced order homogenization for failure analysis of heterogeneous materials. Comput Methods Appl Mech Eng 196(7):1216–1243
44. Pearson JE (1993) Complex patterns in a simple system. Science 261(5118):189–192
45. Polezhaev AA, Pashkov RA, Lobanov AI, Petrov IB (2006) Spatial patterns formed by chemotactic bacteria Escherichia coli. Int J Dev Biol 50(2):309–314
46. Pouya A, Ghoreychi M (2001) Determination of rock mass strength properties by homogenization. Int J Numer Anal Methods Geomech 25(13):1285–1303
47. Sakiyama H, Matsubara H (2018) Physical, chemical, and biological investigation of an unconformity between limestone and sandstone in a coastal area: Iriomote Island case study. CATENA 171:136–144
48. Seifan M, Berenjian A (2019) Microbially induced calcium carbonate precipitation: a widespread phenomenon in the biological world. Appl Microbiol Biotechnol 103(12):4693–4708
49. Shigesada N, Kawasaki K (1997) Biological invasions: theory and practice. Oxford University Press, UK
50. Sun X, Miao L, Tong T, Wang C (2019) Study of the effect of temperature on microbially induced carbonate precipitation. Acta Geotech 14(3):627–638
51. Suzuki K, Kikuchi N (1991) A homogenization method for shape and topology optimization. Comput Methods Appl Mech Eng 93(3):291–318
52. Tang CS, Yin LY, Jiang NJ, Zhu C, Zeng H, Li H, Shi B (2020) Factors affecting the performance of microbial-induced carbonate precipitation (MICP) treated soil: a review. Environ Earth Sci 79(5):1–23
53. Terada K, Kato J, Hirayama N, Inugai T, Yamamoto K (2013) A method of two-scale analysis with micro-macro decoupling scheme: application to hyperelastic composite materials. Comput Mech 52(5):1199–1219
54. Terada K, Kikuchi N (1996) Microstructural design of composites using the homogenization method and digital images. JSMS 45(6Appendix):65–72
55. Terada K, Kikuchi N (2001) A class of general algorithms for multi-scale analyses of heterogeneous media. Comput Methods Appl Mech Eng 190(40–41):5427–5464
56. Terzis D, Laloui L (2018) 3-D micro-architecture and mechanical response of soil cemented via microbial-induced calcite precipitation. Sci Rep 8(1):1–11
57. Terzis D, Laloui L (2019) Cell-free soil bio-cementation with strength, dilatancy and fabric characterization. Acta Geotech 14(3):639–656
58. Thompson JB, Ferris FG (1990) Cyanobacterial precipitation of gypsum, calcite, and magnesite from natural alkaline lake water. Geology 18(10):995–998
59. Tsukamoto Y, Ishihara K, Yamamoto M, Harada K, Yabe H (2000) Soil densification due to static sand pile installation for liquefaction remediation. Soils Found 40(2):9–20
60. Turing AM (1952) The chemical basis of morphogenesis. Bull Math Biol 52(1–2):153–197
61. Whiffin VS, van Paassen LA, Harkes MP (2007) Microbial carbonate precipitation as a soil improvement technique. Geomicrobiol J 24(5):417–423
62. Xiao P, Liu H, Xiao Y, Stuedlein AW, Evans TM (2018) Liquefaction resistance of bio-cemented calcareous sand. Soil Dyn Earthq Eng 107:9–19
63. Yasuda S, Ishihara K, Harada K, Shinkawa N (1996) Effect of soil improvement on ground subsidence due to liquefaction. Soils Found 36(Special):99–107
64. Zhang Y, Guo HX, Cheng XH (2014) Influences of calcium sources on microbially induced carbonate precipitation in porous media. Mater Res Innov 18(sup2):S2-79
65. Zhu T, Dittrich M (2016) Carbonate precipitation through microbial activities in natural environment, and their potential in biotechnology: a review. Front Bioeng Biotechnol 4:4
66. Zienkiewicz OC, Taylor RL, Zhu J (2005) The finite element method: its basis and fundamentals. Elsevier